Supporting Information

Symmons et al. 10.1073/pnas.0900693106

SI Text

Display of Cross-Linking Results. To display the in vivo cross-linking results on the AcrA and AcrB molecular surfaces (Fig. 4*A*) PyMOL (1) coloring commands were used. This approach produces only an approximate representation of the cross-linking propensity on the surfaces. For AcrA the color gradient was: blue within 3.8 Å of the Cβ atom of a mutated residue, through to cyan within 9.0 Å. For mutated residues positive but with a bias to the longer cross-linker: it was green within 3.8 Å, yellow green within 9.0 Å. Finally, for residues that were positive with the short cross-linker it was red within 3.8 Å, through to yellow within 9.0 Å. For AcrB, corresponding distances were slightly increased owing to the greater area exposed i.e., 5.0 Å instead of 3.8 Å, and 12.5 Å instead of 9.0 Å, respectively. This representation cannot take into account the distribution of target lysine residues on the partner protein, which are required for effective cross-linking or the presence of competing lysines on the variant protein itself, which would lead to side reactions giving intramolecular cross-links.

Data-Driven Docking of AcrA and AcrB. The starting structures were the periplasmic domain of AcrB (2) and the partial AcrA structure (3) mutated at seleno-methionine positions to the WT sequence and completed by the homology model of the MP domain deriving from MexA. Cross-linking distances were expressed in CNS-simulated annealing searches (4) as $1/R^6$-weighted ambiguous distance restraints from the Cβ of the mutated residues that were positive in cross-linking experiments to the Nζ of lysine side-chains on the partner protein surface (5). Backbone dihedral angle restraints were relaxed (from ±3° to ±24°) in the interdomain linker regions to allow for domain–domain movements (AcrA linker residues 27–29, 37–40, and 184–187). Docking searches were carried out as CNS-simulated annealing in cartesian mode followed by energy minimization (5,000-K start, 200 steps cooling, 200 steps minimization) starting from AcrA models positioned at random around the periplasmic surface of the AcrB dimer at a range of initial angles. A total of 150 starting positions and models were each run 5 times with random starting atomic trajectories. The final refined model was prepared from a brief further simulated annealing and energy minimization of a solution but with the chemical cross-linking restraints omitted. The linker regions with relaxed dihedral restraints during the docking search were then regularized.

In the cross-linking experiments a number of effects could produce false negatives even when interresidue distances were apparently satisfied, for example, nonfavorable directional effects, steric effects caused by the additional atoms of the cross-linker reagent (which are not included in the refinements), and perhaps most importantly competing reaction with lysine sidechains on the same protein, which will effectively quench the reaction rather than leading to detectable cross-linked products. For these reasons no negative results were included in the original distance requirements, a strategy that has been successful previously (6). However, both positive and negative distances were checked after each refinement by using PyMOL scripts (http://pymolwiki.org), and the results for the final refined solution are shown in Tables S2 and S3. Additional tolerances on cross-linking distances (as specified in *Methods*) were included at this stage to deal with the likely presence of multiple conformers that contribute to the products of the cross-linking reactions. The resolution of the method will be determined by the spread of conformers present in the sample. We obtained a tight cluster of docking results around the final adaptor position of Figs. 4 and 5. If there were additional adaptor positions then we would expect there to be anomalous cross-linking sites outside the expected distances. The resolution of the method therefore is determined by the uncertainty on these distances that were estimated as ±6.0 Å (see *Methods*). Consistent with this, under appropriate conditions we have cases where there is a clear difference between the cross-linking with the short versus the long cross-linking reagents that have linkers differing by a similar length (8.8 Å).

Graphical Display of AcrB Crystal Structure Conformational Variation. During docking only the form corresponding to that of the loose or access (2, 8) conformation was used for the AcrB subunits. This was fixed during the docking and only exposed side chains were allowed to move. To display the regions in the crystallographic structures that are conformationally distinct from the form chosen, a multichain alignment was prepared with LSQMAN (9). This program was used to calculate an optimized superimposition of the 3 chains in coordinate file 2gif.pdb (2), starting from an initial alignment of the residue range 638 to 833. A multi-rmsd was then calculated for each residue, where multi-rmsd = $\sqrt{(d_{12}^2 + d_{13}^2 + d_{23}^2)}/3$, with d_{ij} the distance between the Cα atoms in each (i, j) pair of optimally-superimposed chains. The calculated rmsd values were inserted as pseudo *B* factors for each residue in the A-chain subunit, and then colored by using the color_b.py function (John Campbell, Queens University, Ontario) to show the surface variability as a red–blue color gradient from invariable, blue (< 0.5 Å multi-rmsd) to high variation, red (> 5.0 Å multi-rmsd).

The result of the transporter variation analysis is shown in Fig. S4. By displaying the rmsd values on a molecular surface we obtain an adaptor's eye view of the conformational change involved in the proposed transporter pump mechanism. During docking possible AcrB conformational change in a ±2.5-Å range was allowed for. To check if the docked adaptor comes into contact with regions of substantial conformational change, and which might produce distinct conformations of the adaptor on each subunit, we show the docked solution in Fig. S4 surface as a green ribbon. The blue color of surfaces under the adaptor indicates that it is in contact with regions of the transporter showing relatively little conformational change. The limited change of the surface means that the docked adaptor–transporter subunit model of Fig. 4*B* can be used to generate a symmetrical model of the trimeric AcrB with one adaptor per subunit (gray additions to Fig. S4) for docking to trimeric TolC.

Modeling the Docked TolC–AcrB Interaction. The relative register of the TolC and the AcrB subunits enforced by the cross-linking results is shown in Fig. 5*B*. This docking is one in which the turn from TolC H3 to H4 (indicated by Gly-147) lies adjacent to the AcrB DN subdomain β-hairpin (light blue, marked by Gln-255), but differs from those previously published (10, 11) as it is shifted above the body of the AcrB subunit, rather than overhanging it to the right. Fig. S6 shows a view of the Fig. 5 complex from a different viewpoint to show the resulting contacts in the equivalent TolC H7/H8 and the AcrB DC subdomain interface. If the closed conformation of TolC is applied to this new TolC–AcrB H3/H4 to DN subdomain register deriving from the cross-linking results, then an unfavorable close contact is generated, which is indicated by a red asterisk in Fig. S6*A* between the gray elements representing the crystal structures of the isolated proteins. This unfavorable state can be ameliorated by the movement of the H7/H8 coil (Fig. S6*B*, orange elements marked by Gly-365), which was observed in the partial open-state mutant form (10) and is consistent with an opening mechanism based on closer equivalence of conformation between the two halves of the TolC subunit (12). Likewise, if the equivalence of the N- and C-terminal hemispheres of AcrB were to extend to the conformation of the AcrB β-hairpins then a similar open state of the AcrB DC subdomain β-hairpin conformation (Fig. S6*B*, magenta elements, indicated by Gly-796) can be envisaged. This small conformational change allows the TolC H7/H8 coil turn at Gly-365 to be accommodated adjacent to the DC subdomain (Fig. S6*B*, the position of the AcrB DC β-hairpin is indicated by Gly-740), giving an interface that is equivalent to that between the N-terminal halves of each protein (Fig. S6*B*) and minimizes unfavorable contacts.

1. DeLano WL (2002) *The PyMOL Molecular Graphics System* (DeLano Scientific, Palo Alto, CA).
2. Seeger MA, et al. (2006) Structural asymmetry of AcrB trimer suggests a peristaltic pump mechanism. *Science* 313:1295–1298.
3. Mikolosko J, Bobyk K, Zgurskaya HI, Ghosh P (2006) Conformational flexibility in the multidrug efflux system protein AcrA. *Structure (Structure)* 14:577–587.
4. Brünger AT, et al. (1998) Crystallography and NMR system: A new software suite for macromolecular structure determination. *Acta Crystallogr D* 54:905–921.
5. Lobedanz S, et al. (2007) A periplasmic coiled-coil interface underlying TolC recruitment and the assembly of bacterial drug efflux pumps. *Proc Natl Acad Sci USA* 104:4612–4617.
6. Schulz DM, Ihling C, Clore GM, Sinz A (2004) Mapping the topology and determination of a low-resolution three-dimensional structure of the calmodulin-melittin complex by chemical cross-linking and high-resolution FTICRMS: Direct demonstration of multiple binding modes. *Biochemistry* 43:4703–4715.
7. Qi G, Lee R, Hayward S (2005) A comprehensive and nonredundant database of protein domain movements. *Bioinformatics* 21:2832–2838.
8. Murakami S, Nakashima R, Yamashita E, Matsumoto T, Yamaguchi A (2006) Crystal structures of a multidrug transporter reveal a functionally rotating mechanism. *Nature* 443:173–179.
9. Kleywegt GJ (1996) Use of noncrystallographic symmetry in protein structure refinement. *Acta Crystallogr D* 52:842–857.
10. Bavro VN, et al. (2008) Assembly and channel opening in a bacterial drug efflux machine. *Mol Cell* 30:114–121.
11. Fernandez-Recio J, et al. (2004) A model of a transmembrane drug-efflux pump from Gram-negative bacteria. *FEBS Lett* 578:5–9.
12. Koronakis V, Sharff A, Koronakis E, Luisi B, Hughes C (2000) Crystal structure of the bacterial membrane protein TolC central to multidrug efflux and protein export. *Nature* 405:914–919.
13. Gouet P, Robert X, Courcelle E (2003) ESPript/ENDscript: Extracting and rendering sequence and 3D information from atomic structures of proteins. *Nucleic Acids Res* 31:3320–3323.
14. Higgins MK, Bokma E, Koronakis E, Hughes C, Koronakis V (2004) Structure of the periplasmic component of a bacterial drug efflux pump. *Proc Natl Acad Sci USA* 101:9994–9999.

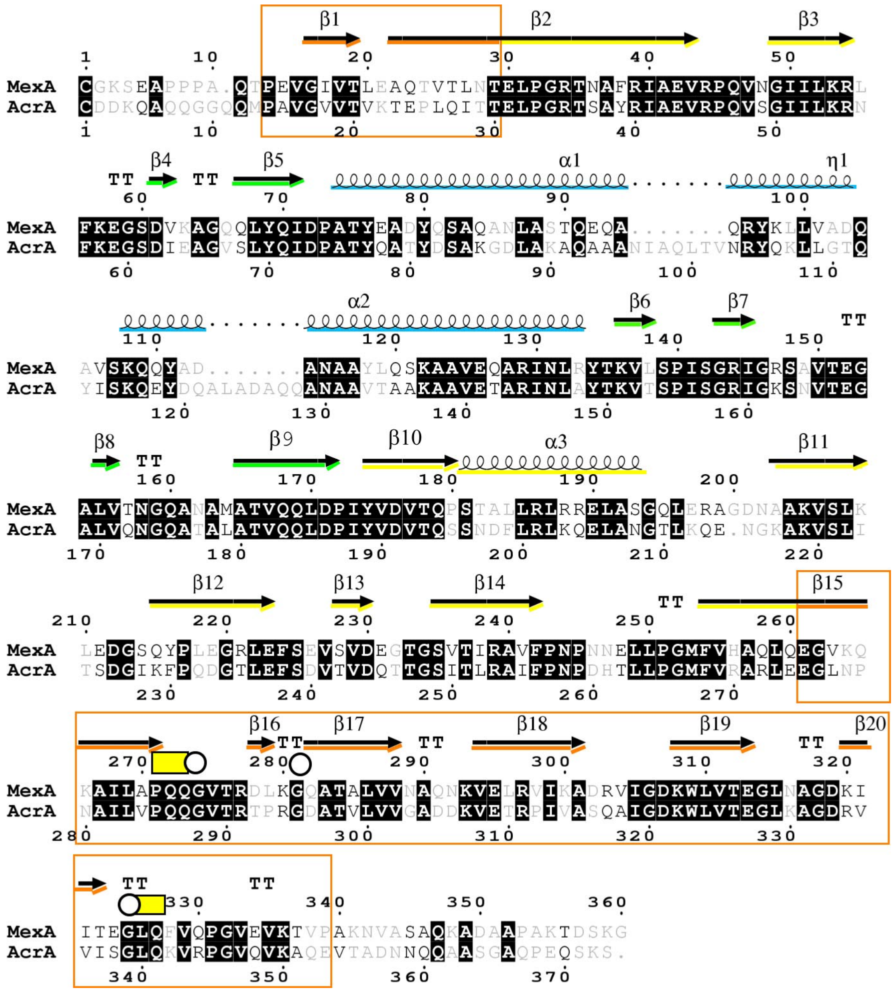

Fig. S1. Homology of MexA and AcrA adaptors. The *P. aeruginosa* MexA sequence is aligned to that of *E. coli* AcrA, with secondary structural elements, highlighted in the same domain colors as in Fig. 2*A*, annotated by Espript (13). Sequence numbering is for mature proteins with the signal peptides removed. Identity in sequence is highlighted, conservative replacement in black, nonconserved residues in gray. Orange boxing indicates the extent of the new MP domain elements traced in the re-refinement of the MexA structure (see Table S1). Conserved Gly residues in the MP domain presented in Figs. 2 and 4 as white Cα atoms are marked by white circles above the sequence, and the adjacent helical turns in the MP domain are similarly indicated by yellow blocks.

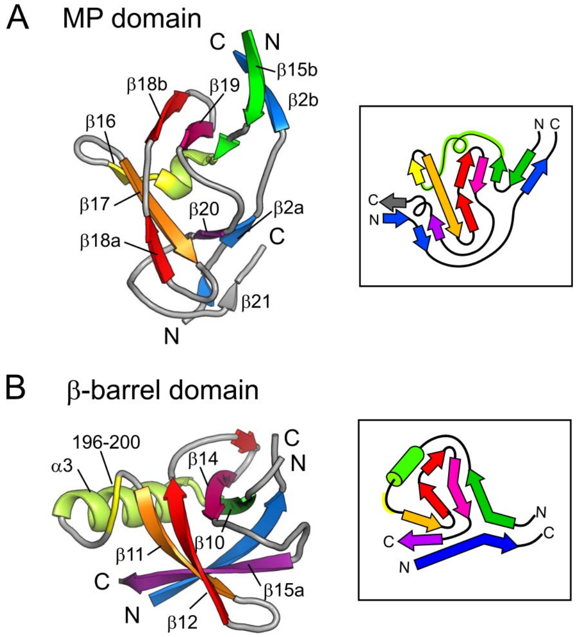

Fig. S2. Comparing adaptor MP and β-barrel domain topologies. The topology of the MexA MP domain (shown in Fig. 2*A*) is here compared with that of the β-barrel domain from a different viewpoint. (*A*) The overall β-roll topology with the β-ribbon linker shown top right and colored as in Fig. 2*A Inset*. The N-terminal strand (blue elements) passes through the domain and then contributes to this β-ribbon linker. The C-terminal linker strand passes into the domain as a short initial strand (β15b) and then a first helical turn motif (PQQ). The core of the domain is a β-meander element (β16, β17, β18a; yellow, orange, red). A β-hairpin (β18b, β19; red, magenta) is folded back over the top of this meander, followed by an extended S-shaped linker (β19 to β20, residues 314–319) and then a second helical turn motif. The resulting topology is depicted in the *Inset*. (*B*) The structure and an equivalent topological analysis (*Inset*) of the MexA β-barrel domain indicating the overall similarity to the MP domain. Comparing the topology of the β-barrel with that of the MP β-roll shows the equivalence of the S-shaped linker between the β-barrel β14 and β15a to that between the MP β19 and β20. The principle differences between the domains arise from extension of some secondary structural elements that allows the complete β-barrel to form. In addition, the β-barrel has a true α-helical element (α3) instead of the helical PQQ turn. The length of this α3 helix is such that the structural equivalent of the MP β16 strand is, in the β-barrel, subsumed into the turn (residues 198–200, yellow) between α3 and β11.

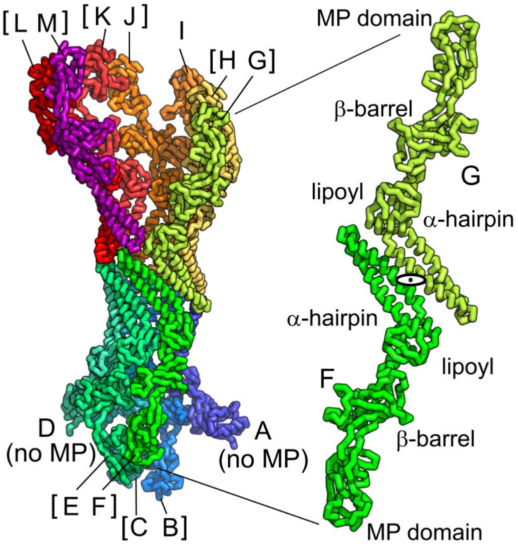

Fig. S3. Arrangement of multiple copies of the complete MexA in the crystal ASU. Cα trace of MexA chains in the re-refined monoclinic crystal ASU. Each of the 13 chains is represented in a color on a blue to red spectrum and labeled A-M. MP domains could not be modeled in the A and D chains. Pairing of other MP domains (except for chain I) are indicated by square brackets around chain designations. Central antiparallel pairing of coiled-coil of chain F and G α-hairpin domains is shown enlarged to the right. This is significant as a structurally very similar antiparallel pairing of the adaptor α-hairpin with the TolC H3/H4 coiled-coil was produced by the re-optimized docking (Fig. 5*B*).

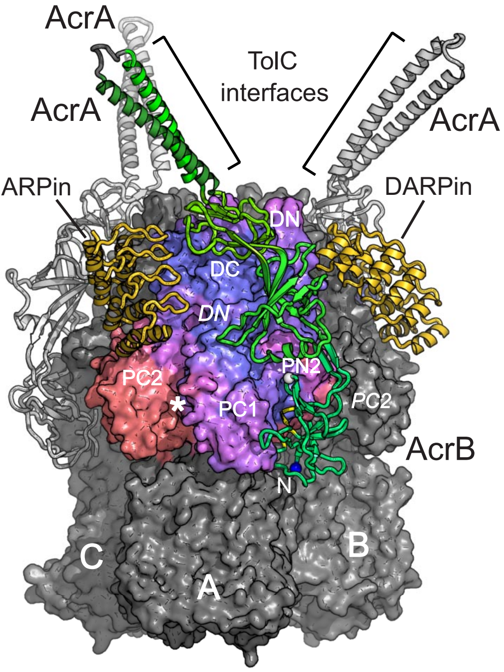

Fig. S4. Adaptor and DARPin positions compared with transporter surface variation. The surface of one AcrB subunit is colored on a blue (low) to red (high) gradient of backbone conformational variation among the three transporter subunits [calculated as a multi-RMSD (9) as described in *SI Text*]. The membrane region is in gray. The docked AcrA protein is shown in green on the colored surface and positions on the other two subunits are shown in gray. AcrB subdomains are labeled with subdomains on adjacent subunits (italicized). Also shown are the binding sites of two artificial DARPin inhibitors (gold ribbon) on this completed trimeric model with docked adaptors. Comparing the bound DARPins and the docked adaptors shows that there is no clash between their positions. The DARPins bind to a region centered on the DC subdomain with contacts to the upper edge of PC2. The red color of the PC2 surface indicates that it undergoes a large conformational change during the postulated pump mechanism. Indeed, the changes in the cleft between PC2 and PC1 (marked by a white asterisk on the surface) have been proposed to regulate substrate (drug) access to the pump. Also shown in the trimeric state is that the PC2 subdomain of an adjacent AcrB subunit (gray domain labeled PC2 in italics) is positioned next to the MP domain but does not contact it. The inward directed TolC binding surfaces of AcrA adaptors are marked.

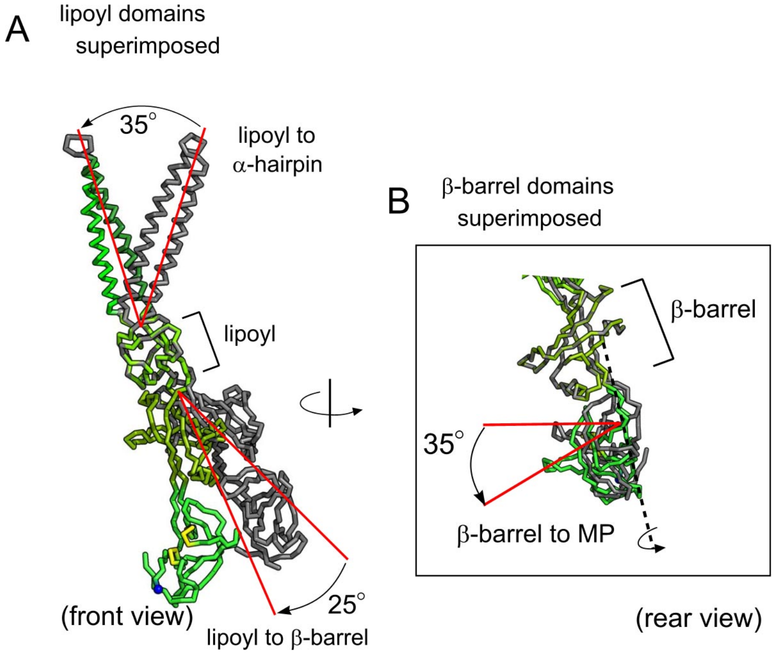

Fig. S5. Adaptor conformational change from crystal form to docked state. The successful docking of the AcrA adaptor required significant interdomain movements as it approached the AcrB transporter surface. To reveal these movements 2 superimpositions were produced of the final docked conformation onto the original crystal form. (*A*) A view of the docked conformation (green) compared with the crystal form (gray) by superimposing their lipoyl domains. This view presents the concave face of the MP domain (indicated by the yellow helical turns). The hinge-like movements of both the β-barrel downward relative to the lipoyl domain (an angle of 25°) and the α-hairpin in a vertical plane above the lipoyl domain (elbowed through a 35° angle) are marked. The specific MP domain conformational change is masked by the large β-barrel movement. (*B*) A different superimposition to reveal this MP domain reorientation. Here, the β-barrel domains of the docked and crystal forms are superimposed and then viewed from the back to show the convex face of the MP domain. This reveals a 35° rotation, relative to the β-barrel, around the vertical axis of the β-linker of the MP domain. These angles are comparable to known examples of conformational change documented in structural databases (7) and here, in addition to satisfying the experimental cross-linking distance restraints, allow favorable contacts between the domains of the adaptor and the AcrB transporter surface.

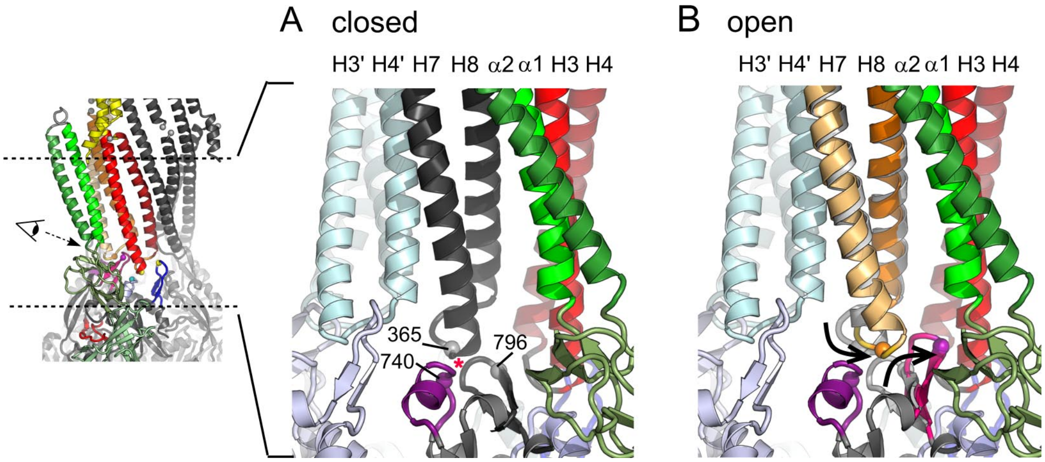

Fig. S6. Open-state modeling. The TolC–AcrB interface, shown in Fig. 5*B*, indicated between the thumbnail dotted lines to the right is viewed from the direction shown by the eye symbol to illustrate the detail of the docking. (*A*) The result of the TolC–AcrB register, enforced by the cross-linking results, when the crystal forms of the proteins are used (2, 12). The red asterisk shows the resulting close contact between the TolC H7-H8 turn (the latter indicated here by the residue 365 Cα atom) and the AcrB β-hairpin (indicated by the residue 796 Cα). (*B*) Shown is how this close contact can be ameliorated by using the TolC partially open state mutant (ref. 10, orange turn and 365 Cα atom) and then imposing a vertical conformation on the AcrB DC subdomain β-hairpin (shown as a magenta turn and 796 Cα). Arrows indicate these 2 conformational adjustments. The α-helices at the interface are colored as for Fig. 5*B* and are labeled along the top. An adjacent AcrB-TolC subunit interface is now visible to the left and shown in light blue-pale cyan (adjacent TolC helices labeled H3′ and H4′).

Table S1. MexA monoclinic crystal re-refinement statistics

Crystallographic data summary	
Space group	P 2_1
a (Å)	130.55
b (Å)	213.31
c (Å)	183.58
β (°)	107.4
Resolution range (last shell) (Å)	65.6–3.2 (3.4- 3.2)
Total no. reflections (last shell)	156 400 (25 928)
Completeness (last shell) (%)	98.9 (98.9)
Re-refinement statistics	
R_{work} (R_{free}) (%)	23.9 (26.4)
Maximum-likelihood coordinate error (Å)	0.43
Total no. atoms	
Protein (residues)	28 523 (4059)
Solvent (sulphates)	80 (16)
Geometry	
ΔBonds (Å)	0.008
ΔAngles (°)	1.2
Wilson *B* factor	66.7
Average *B* factor all atoms (Å^2)	71.7
Total no. NCS restraint groups over 13 chains	63
Residues in favored, allowed, disallowed regions of Ramachandran plot (%)	89.4, 99.1, 0.9
F-chain only analysis	
Average *B* factor all atoms (Å^2)	74.7
Residues in sequence	360 (1–360)
Total no. residues in starting model (sequence range)	231 (29–259)
Total no. residues in new model (sequence range)	327 (13–339)
Residues truncated to Ala in model (% of all model)	27 (8%)

Statistics for re-refined MexA model after tight NCS restrained geometric refinement in CNS 1.1 followed by restrained *B*-factor refinement with PHENIX 1.3. Crystallization details and intensity statistics remain as published (14).

Table S2. Distances between cross-linked residues in refined AcrA-AcrB docked model

Cross-linked Cys residues	Distance to closest Lys, Å
AcrA	
E31C (S)	12.5 (K226*)
K58C (S)	10.9 (K778)
A65C (L)	19.7 (K195)
E167C (L)	14.7 (K195)
T177C (L)	17.0 (K778)
S196C (S)	10.7 (K589)
D226C (S)	5.9 (K267)
D296C (S)	11.9 (K632)
D321C(S)	10.0 (K322)
E327C(L)	19.5 (K603)
S338C(S)	11.9 (K334)
Q352C(S)	12.0 (K334)
AcrB	
L25C (L)	21.5 (K342)
D153C (S)	13.6 (K229)
K226C (S)	12.6 (K162)
R259C (S)	13.0 (K58)
K267C (S)	10.6 (K58)
Q284C (S)	8.5 (K322)
A304C (S)	10.5 (K342)

Modeled cross-link distances are shown for either AcrA or AcrB residues giving positive reaction with either S or L cross-linker (Fig. 3). Predicted partner Lys is shown in parentheses alongside distance. Short distance is taken as 8.8 ±6.0 Å from the mutated Cβ atom to Nζ atom of Lys; long distance taken as 17.6 ±6.0 Å (see *Methods*). Asterisked lysine is on DN subdomain from adjacent subunit of AcrB trimer. Analysis of closest cross-linkable Lys residues excludes those that are less than the minimum distance.

Table S3. Distances in refined docked AcrA-AcrB model for noncross-linked Cys residues

Cys residues	Distance to closest Lys, Å
AcrA	
Q27C	16.1 (K334)
L53C	18.0 (K735)
S239C	17.5 (K226*)
Q245C	*9.4 (K589)*
D260C	*13.9 (K267)*
L264C	*10.3 (K267)*
E274C	19.7 (K226*)
L277C	19.8 (K322)
K330C	15.2, (K322)
AcrB	
R586C	20.0 (K203)
E641C	26.9 (K342)
Q701C	26.7 (K22)
H709C	31.1 (K22)
S715C	38.4, (K342) 38.5 (K350*)
K735C	23.7 (K54) 23.9 (K58*)
D784C	*7.0 (K162)*
R808C	20.8 (K162)
T853C	16.6 (K22)

Modeled distances are shown for either AcrA or AcrB residues that did not give observed cross-links (Fig. 3). Direct distance to the nearest Lys on the partner protein is shown with residue in parentheses. Distances as in Table S2 (see *Methods*). Italicized results are negative anomalies that appear to be within the shorter distance but give no cross-linking. More of the negatives are within the longer cross-linking distance but the occurrence of long-only reaction appears generally disfavored by a factor of ≈10 (based on all of our results with the method to date). This may be caused by quenching as described. Asterisked lysines are from adjacent subunits of AcrB trimer.

Table S4. Distances between cross-linked residues in reoptimized AcrA α-hairpin to TolC docked model

Cys residues	Distance to closest Lys, Å
AcrA	
A75C (L)	16.9 (K383)
A79C (S)	11.1 (K383)
D87C (S)	6.6 (K383)
L100C (S)	13.6 (K401)
R104C (S)	8.5 (K401)
Q112C (S)	9.7 (K401)
I114C (L)	14.5 (K218)
E118C (S)	8.9 (K401)
TolC	
S124C (S)	6.8 (K85)
Q139C (S)	7.6 (K54)
Q142C (S)	3.7 (K54)
S363C (S)	14.1 (K54)

Modeled cross-link distances are shown for either AcrA or TolC residues giving positive reaction with either S or L cross-linker (5). Predicted partner Lys is shown in parentheses alongside distance. Distances as in Table S2 (see *Methods*).